Check for updates

A SFBEM–FEM coupling method for solving crack problems based on Erdogan fundamental solutions

Cheng Su[1,2,3] · Kemin Cai[1] · Zhi Xu[1]

Abstract

The boundary element method (BEM) has proven to be an efficient approach for crack analysis in fracture mechanics, while its versatility in application to crack problems of complex structures with irregular boundaries deserves further attention. In this study, to improve the applicability to complex crack analysis, a cracked superelement is first established with BEM to model the near-crack region, and the crack problem is then solved within the frame of finite element method (FEM). The stiffness matrix of the cracked superelement is formulated using the spline fictitious boundary element method (SFBEM) based on the Erdogan fundamental solutions for an infinite plane with a single crack. The proposed superelement is further incorporated into a finite element mesh to simulate the behaviour of the crack zone, and the governing equation of the crack problem is finally established and solved using the typical procedure of FEM. After obtaining the nodal displacements of the superelement, the stress intensity factors (SIFs) of crack tips can be obtained by a backward analysis with SFBEM. The accuracy and efficiency of the proposed SFBEM–FEM coupling method are demonstrated by two numerical examples involving a rectangular plate with a central crack and a square plate with 100 horizontal cracks. The present approach is further applied to the analysis of the SIFs of multiple cracks exposed in a steel anchorage box for a hanger of a suspension bridge, which indicates the merging of the cracked superelements to the commercial FEM software is computationally efficient for the analysis of complex structures with multiple cracks.

✉ Cheng Su
 cvchsu@scut.edu.cn

[1] School of Civil Engineering and Transportation, South China University of Technology, Guangzhou 510640, China

[2] State Key Laboratory of Subtropical Building Science, South China University of Technology, Guangzhou 510640, China

[3] Guangdong Artificial Intelligence and Digital Economy Laboratory, Guangzhou 510335, China

1 Introduction

The analysis of stress intensity factors (SIFs) is of great importance to the assessment of damage tolerance and the prediction of crack propagation for engineering structures. As analytical methods are generally limited to solving simple crack problems [1], various numerical methods, e.g. the finite element method (FEM) [2], the extended finite element method (XFEM) [3] and the boundary element method (BEM) [4], have been developed for analysis of SIFs in engineering practice. Due to its high flexibility in modelling complex structures and imposing complex boundary conditions, the FEM is the most commonly used numerical method for solving crack problems of engineering structures. However, because of the crack-tip singularity, mesh refinement is required at crack tips so as to capture the singular behaviour of stresses, leading to extra burden of mesh generation and large computational cost of FEM for crack problems. The XFEM alleviates the shortcomings of the traditional FEM associated with mesh refinement of crack regions, in which local enrichment functions consisting of a discontinuous function and the near-tip asymptotic fields are incorporated into finite element formulation to describe the jump in displacement across the crack surface and the singularity at the crack tip, resulting in extra degrees-of-freedom (DOFs) in XFEM for crack problems [5, 6].

As an alternative to FEM, the BEM has proven to be a powerful numerical method to solve crack problems, in which only boundary rather than domain discretization is required for analysis of SIFs. The existing BEMs applied to crack problems can be roughly classified into two categories depending on the fundamental solutions used. For the first category, the Kelvin fundamental solutions [7] for noncrack problems are adopted in the formulation of BEM, in which the stress boundary conditions along crack surfaces need to be satisfied and special boundary elements are required at crack tips to reflect the singular behaviour [8, 9]. For the second category, the Erdogan fundamental solutions [10] for crack problems are employed in the BEM formulation [11–13], in which the stress boundary conditions on the crack surfaces are automatically satisfied and the singular behaviour at crack tips can be naturally reflected. Therefore, there is no need to set boundary elements on the crack surfaces, and furthermore, the SIFs of the crack tips can be calculated directly using the specific fundamental solutions of SIFs.

However, for crack problems of complex structures with complex boundary conditions, it is not convenient to model the structures and apply the boundary conditions with BEM, and for multi-crack problems, multi-domain coupling techniques are further required in BEM formulation when the single-crack Erdogan fundamental solutions are used. Therefore, in order to make full use of the unique advantage of BEM in dealing with the singular behaviour at crack tips and the superior flexibility of FEM in modelling complex structures and boundary conditions, several researchers proposed the BEM–FEM coupling methods to solve complex crack problems [14–18].

Actually, the coupling method based on boundary discretization methods and FEM stems from the pioneering work of Zienkiewicz et al. [19] and Brebbia and Georgiou [20], and now have appeared in the areas of flexoelectricity [21], vibroacoustic response [22–24], fluid–structure interaction [25] and soil–structure interaction [26], among others. Note that, for crack problems thus far, the BEM formulation for the BEM subdomain containing cracks has been established using the noncrack Kelvin fundamental solutions, and therefore, one also needs to consider the stress boundary conditions on crack surfaces and employ special crack-tip boundary elements to reflect the singular behaviour, which makes it inconvenient to calculate the SIFs at crack tips, even if the coupled BEM–FEM procedure has been adopted.

In this study, a coupled BEM–FEM procedure is developed for the analysis of complex structures in the presence of cracks. The near-crack region is modelled as a cracked superelement, and its stiffness matrix is formulated with the spline fictitious boundary element method (SFBEM) [27–29], in which, to automatically satisfy the stress boundary conditions on crack surfaces and naturally capture the crack-tip singularity, the Erdogan fundamental solutions corresponding to an infinite cracked plane are employed instead of the traditional noncrack Kelvin fundamental solutions. For the other regions without cracks, the conventional finite elements are used to model the structure. Then, the proposed stiffness formulation of the cracked superelement can be assembled to the global finite element formulation, from which the nodal displacements of the structure, including those of the superelement, can be obtained following the typical FEM procedure. After obtaining the nodal displacements of the superelement, the SIFs of the crack tips can be readily obtained by a backward analysis with SFBEM focussing on the domain of the superelement. As the SIF fundamental solutions are known in advance as a part of the Erdogan fundamental solutions, the crack-tip SIFs can be calculated directly based on the superposition of the SIF fundamental solutions in the above backward analysis. The accuracy and efficiency of the proposed SFBEM–FEM coupling method are demonstrated by numerical examples involving a rectangular plate with a central crack and a square plate with 100 horizontal cracks. The present approach is further applied to the analysis of a multi-crack steel anchorage box for a hanger of a suspension bridge, indicating the wide applicability of the SFBEM–FEM coupling method to complex crack problems.

2 Formulation of stiffness matrix for cracked superelement by SFBEM

As the Erdogan fundamental solutions [10] for crack problems are derived by the method of complex variable function and expressed in a more complicated manner, it is more advantageous to employ SFBEM, a nonsingular indirect BEM, for the analysis of the cracked domain, in which singular integrals of the complex fundamental solutions are completely avoided [11–13]. In this section, the Erdogan fundamental solutions are first presented, and the stiffness matrix of the cracked superelement is then formulated using SFBEM.

Fig. 1 Concentrated loads in an infinite plane with a crack
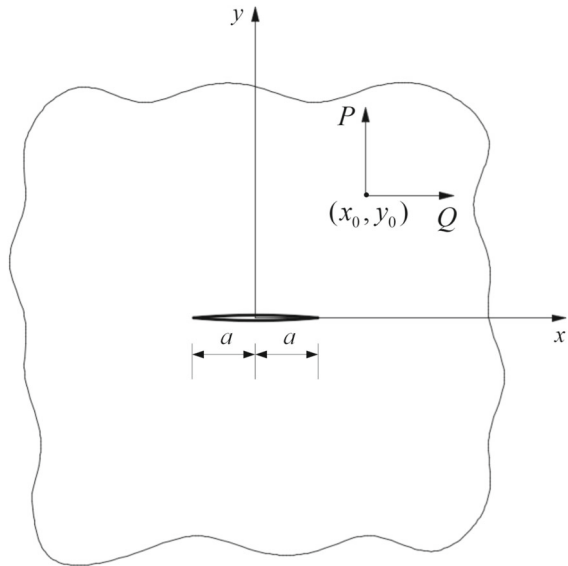
2.1 Erdogan fundamental solutions for plane crack problems

Consider an infinite cracked plane subjected to concentrated forces Q and P at an arbitrary source point $z_0 = x_0 + iy_0$, as shown in Fig. 1. The complex variable stress functions are taken as follows:

$$
\left.
\begin{aligned}
\phi(z) &= -\frac{S}{z-z_0} + \phi_0(z) \\
\Omega(z) &= \frac{\kappa S}{z-\bar{z}_0} + \frac{\bar{S}(\bar{z}_0-z_0)}{(z-\bar{z}_0)^2} + \phi_0(z) \\
\phi_0(z) &= \frac{1}{2\pi\sqrt{z^2-a^2}}\left\{ \frac{S}{z-z_0}[I(z)-I(z_0)] - \frac{\kappa S}{z-\bar{z}_0}[I(z)-I(\bar{z}_0)] \right. \\
&\quad \left. -\bar{S}(\bar{z}_0-z_0)\left[\frac{I(z)-I(\bar{z}_0)}{(z-\bar{z}_0)^2} - \frac{J(\bar{z}_0)}{z-\bar{z}_0}\right]\right\}
\end{aligned}
\right\}, \tag{1}
$$

where

$$
\left.
\begin{aligned}
I(z) &= \pi\left(\sqrt{z^2-a^2}-z\right) \\
J(z) &= \pi\left(\frac{z}{\sqrt{z^2-a^2}}-1\right) \\
S &= \frac{Q+iP}{2\pi(1+\kappa)} \\
\kappa &= \begin{cases} 3-4\upsilon & \text{(Plane strain)} \\ \frac{3-\upsilon}{1+\upsilon} & \text{(Plane stress)} \end{cases}
\end{aligned}
\right\}. \tag{2}
$$

In the above equations, $z = x + iy$ denotes an arbitrary field point; a is the half crack length; and υ is the Poisson's ratio of the material.

The stresses σ_x^0, σ_y^0 and τ_{xy}^0 and the displacements u_x^0 and u_y^0 at any point $z=x+\mathrm{i}y$ are derived from the stress functions and can be expressed as

$$\left.\begin{array}{l} \sigma_x^0 + \sigma_y^0 = 2[\phi(z) + \overline{\phi(z)}] \\ \sigma_y^0 - \sigma_x^0 + 2\mathrm{i}\tau_{xy}^0 = 2[(\bar{z} - z)\phi'(z) - \phi(z) + \overline{\Omega(z)}] \end{array}\right\}, \tag{3}$$

$$2\mu(u_x^0+\mathrm{i}u_y^0) = \kappa \int_0^z \phi(z)\mathrm{d}z - \int_0^{\bar{z}} \Omega(\bar{z})\mathrm{d}\bar{z} + (\bar{z} - z)\overline{\phi(z)}, \tag{4}$$

where the superscript 0 denotes the responses are caused by Q and P applied at $z_0 = x_0 + \mathrm{i}y_0$; the barred quantities are the complex conjugates; the primed quantities represent the derivatives with respect to z; and μ is the shear modulus of the material.

It can be seen from Eqs. (1)–(3) that the stresses are singular at the point of concentrated forces, that is, the stresses become infinite as z approaches z_0. The stresses also become infinite as z approaches $\pm a$, having the required square root singularity at the crack tips.

Accordingly, the SIFs for the crack tips can be further derived as

$$\begin{aligned} K^0 &= K_\mathrm{I}^0 - \mathrm{i}K_\mathrm{II}^0 = 2\sqrt{2\pi} \lim_{z\to\pm a} \left[(\sqrt{z\mp a})\phi(z) \right] \\ &= \frac{\pm 1}{2(1+\kappa)\sqrt{\pi a}} \left\{ (Q+\mathrm{i}P) \left[\left(\frac{z_0\pm a}{\sqrt{z_0^2-a^2}} - 1 \right) - \kappa \left(\frac{\bar{z}_0\pm a}{\sqrt{\bar{z}_0^2-a^2}} - 1 \right) \right] \pm \frac{a(Q-\mathrm{i}P)(\bar{z}_0-z_0)}{(\bar{z}_0\mp a)\sqrt{\bar{z}_0^2-a^2}} \right\}, \end{aligned} \tag{5}$$

where K_I^0 and K_II^0 are the SIFs of model-I and model-II, respectively.

Let $P = 0$, $Q = 1$ or $P = 1$, $Q = 0$ in Eqs. (1)–(5). Then, the above solutions become the Erdogan fundamental solutions for plane crack problems, which can be denoted as $G_{\sigma_x}^{(k)}(z; z_0)$, $G_{\sigma_y}^{(k)}(z; z_0)$, $G_{\tau_{xy}}^{(k)}(z; z_0)$, $G_{u_x}^{(k)}(z; z_0)$, $G_{u_y}^{(k)}(z; z_0)$, $G_{K_\mathrm{I}}^{(k)}(z_0)$ and $G_{K_\mathrm{II}}^{(k)}(z_0)(k = 1, 2)$, with $k = 1$ when $P = 0$, $Q = 1$ and $k = 2$ when $P = 1$, $Q = 0$.

2.2 Stiffness matrix of cracked superelement

Consider an arbitrary cracked superelement Ω_e with a contour L and with a total number of N nodes, as shown in Fig. 2, in which the crack is on the x-axis and its length is taken as $2a$ and a for an inner crack and an edge crack, respectively. In order to establish the stiffness matrix of the cracked superelement, assume that the nodal displacements $U_{x,n}$ and $U_{y,n}(n = 1, 2, \ldots, N)$ are known, and the nodal forces $F_{x,n}$ and $F_{y,n}(n = 1, 2, \ldots, N)$ are required to be determined from the nodal displacements, which is actually a displacement boundary value problem and can be solved by SFBEM.

Embed the cracked superelement into an infinite plane, and apply unknown fictitious loads $X^{(k)}(k = 1, 2)$ along a fictitious boundary S outside Ω_e, whose shape is similar to that of the real boundary L, as also shown in Fig. 2. Then, under the action of the fictitious loads $X^{(k)}(k = 1, 2)$, the displacements and stresses at any point $z=x+\mathrm{i}y$ in the infinite plane can be expressed as
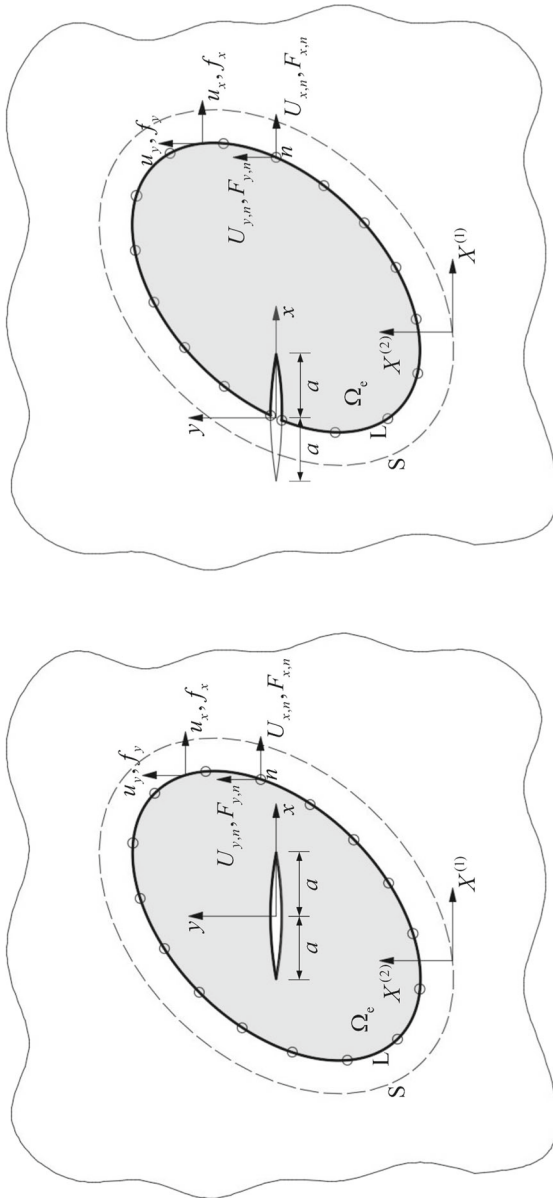
Fig. 2 Cracked superelement embedded in an infinite plane

(a) inner crack

(b) edge crack

$$\left. \begin{aligned} u_x(z) &= \sum_{k=1}^{2} \int_S G_{u_x}^{(k)}(z; z_S) X^{(k)}(z_S) ds \\ u_y(z) &= \sum_{k=1}^{2} \int_S G_{u_y}^{(k)}(z; z_S) X^{(k)}(z_S) ds \end{aligned} \right\}, \tag{6}$$

$$\left. \begin{aligned} \sigma_x(z) &= \sum_{k=1}^{2} \int_S G_{\sigma_x}^{(k)}(z; z_S) X^{(k)}(z_S) ds \\ \sigma_y(z) &= \sum_{k=1}^{2} \int_S G_{\sigma_y}^{(k)}(z; z_S) X^{(k)}(z_S) ds \\ \tau_{xy}(z) &= \sum_{k=1}^{2} \int_S G_{\tau_{xy}}^{(k)}(z; z_S) X^{(k)}(z_S) ds \end{aligned} \right\}, \tag{7}$$

where $z_S \in S$; and $G_{u_x}^{(k)}$, $G_{u_y}^{(k)}$, $G_{\sigma_x}^{(k)}$, $G_{\sigma_y}^{(k)}$ and $G_{\tau_{xy}}^{(k)}(k = 1, 2)$ are the Erdogan fundamental solutions of plane crack problems presented in Sect. 2.1.

Because of using the Erdogan fundamental solutions, the stresses shown in Eq. (7) automatically satisfy both the governing differential equations within Ω_e and the stress boundary conditions on the crack surface. Therefore, only the displacement boundary conditions along the contour L for the cracked superelement need to be considered.

Substituting Eq. (6) into the displacement boundary conditions along L, one has

$$\left. \begin{aligned} \sum_{k=1}^{2} \int_S G_{u_x}^{(k)}(z_L; z_S) X^{(k)}(z_S) ds &= u_x(z_L) \\ \sum_{k=1}^{2} \int_S G_{u_y}^{(k)}(z_L; z_S) X^{(k)}(z_S) ds &= u_y(z_L) \end{aligned} \right\}, \tag{8}$$

where $z_L \in L$; and $u_x(z_L)$ and $u_y(z_L)$ are the known displacement functions along L, which can be expressed as

$$\left. \begin{aligned} u_x(z_L) &= \sum_{n=1}^{N} \eta_n(z_L) U_{x,n} \\ u_y(z_L) &= \sum_{n=1}^{N} \eta_n(z_L) U_{y,n} \end{aligned} \right\}, \tag{9}$$

where $U_{x,n}$ and $U_{y,n}(n = 1, 2, \ldots, N)$ are the known nodal displacements; and $\eta_n(n = 1, 2, \ldots, N)$ are the displacement interpolation functions. In this study, the boundary displacements are determined by linear interpolation from two adjacent nodal displacements.

As the source point z_S and the field point z_L are located on the fictitious boundary S and the real boundary L, respectively, the integral equations shown in Eq. (8) are nonsingular fictitious boundary integral equations, which need to be solved on a numerical basis. For this purpose, the unknown fictitious loads $X^{(k)}(k = 1, 2)$ are expressed in terms of a set of B-spline functions as follows [11, 27]:

$$X^{(k)}(z_S) = \sum_{i=-1}^{N_S+1} x_i^{(k)} \varphi_i(z_S) \ (k = 1, 2), \tag{10}$$

where N_S is the number of fictitious boundary elements; $x_i^{(k)}(i = -1, 0, \ldots, N_S + 1)$ are the unknown spline node parameters; and $\varphi_i(z_S)(i = -1, 0, \ldots, N_S + 1)$ are B-spline functions of the third order.

Substituting Eq. (10) into Eq. (8), one obtains the residual functions along boundary L as follows:

$$
\left.
\begin{array}{l}
R_{u_x}(z_L) = \sum\limits_{k=1}^{2} \sum\limits_{i=-1}^{N_S+1} x_i^{(k)} \int_S G_{u_x}^{(k)}(z_L; z_S)\varphi_i(z_S)\mathrm{d}s - u_x(z_L) \\[2ex]
R_{u_y}(z_L) = \sum\limits_{k=1}^{2} \sum\limits_{i=-1}^{N_S+1} x_i^{(k)} \int_S G_{u_y}^{(k)}(z_L; z_S)\varphi_i(z_S)\mathrm{d}s - u_y(z_L)
\end{array}
\right\}.
\tag{11}
$$

To eliminate boundary residues $R_{u_x}(z_L)$ and $R_{u_y}(z_L)$, divide boundary L into N_L segments, and let the integrals of the residues along each segment equal zero, namely,

$$
\left.
\begin{array}{l}
\int_{\Delta L_j} R_{u_x}(z_L)\mathrm{d}l = 0 \\[1.5ex]
\int_{\Delta L_j} R_{u_y}(z_L)\mathrm{d}l = 0
\end{array}
\right\} \quad (j = 1, 2, \ldots, N_L),
\tag{12}
$$

where ΔL_j is the jth segment on boundary L.

Substitution of Eqs. (9) and (11) into Eq. (12) yields

$$
A_U X = H U_e,
\tag{13}
$$

where X is the unknown vector consisting of the spline node parameters $x_i^{(k)}(i = -1, 0, \ldots, N_S + 1)$ of the fictitious loads along S; A_U is the influence matrix of X depending on the nonsingular integrals of the Erdogan fundamental solution multiplied by the B-spline function; $U_e = [U_{x,1}U_{y,1}U_{x,2}U_{y,2} \cdots U_{x,N}U_{y,N}]^T$ is the nodal displacement vector of the cracked superelement; and H is the matrix depending on the integrals of the displacement interpolation functions.

Generally, overdeterminate collocation is employed to achieve a better solution with more boundary segments while keeping the number of fictitious boundary elements at a lower level. Therefore, Eq. (13) needs to be solved on a least-squares basis as follows [27]:

$$
X = A_U^+ H U_e,
\tag{14}
$$

where

$$
A_U^+ = (A_U^T A_U)^{-1} A_U^T.
\tag{15}
$$

Once the unknown spline node parameters $x_i^{(k)}(i = -1, 0, \ldots, N_S+1)$ are obtained from Eq. (14), the responses of the cracked superelement can be readily calculated from the fictitious loads $X^{(k)}(k = 1, 2)$ shown in Eq. (10). In particular, to obtain the

nodal forces $F_{x,n}$ and $F_{y,n}(n = 1, 2, \ldots, N)$ shown in Fig. 2, the surface loads f_x and f_y along L need to be determined from Eq. (7), which can be expressed as

$$\left. \begin{aligned} f_x(z_L) = n_x\sigma_x(z_L) + n_y\tau_{xy}(z_L) = \sum_{k=1}^{2} \int_S \left[n_x G_{\sigma_x}^{(k)}(z_L;z_S) + n_y G_{\tau_{xy}}^{(k)}(z_L;z_S) \right] X^{(k)}(z_S)ds \\ f_y(z_L) = n_x\tau_{xy}(z_L) + n_y\sigma_y(z_L) = \sum_{k=1}^{2} \int_S \left[n_x G_{\tau_{xy}}^{(k)}(z_L;z_S) + n_y G_{\sigma_y}^{(k)}(z_L;z_S) \right] X^{(k)}(z_S)ds \end{aligned} \right\}, \tag{16}$$

where n_x and n_y are the cosine functions of normal vector for boundary L.

Then, the nodal forces $F_{x,n}$ and $F_{y,n}(n = 1, 2, \ldots, N)$ can be obtained from the surface loads f_x and f_y using the static equivalent principle, which can be expressed as

$$\left. \begin{aligned} F_{x,n} = \int_L \eta_n(z_L) f_x(z_L)dl \\ F_{y,n} = \int_L \eta_n(z_L) f_y(z_L)dl \end{aligned} \right\} (n = 1, 2, \ldots, N), \tag{17}$$

where $\eta_n(n = 1, 2, \ldots, N)$ are the displacement interpolation functions adopted in Eq. (9).

Substituting Eqs. (10) and (16) into Eq. (17) yields

$$F_e = A_F X, \tag{18}$$

where $F_e = [F_{x,1} F_{y,1} F_{x,2} F_{y,2} \cdots F_{x,N} F_{y,N}]^T$ is the nodal force vector of the cracked superelement; and A_F is the influence matrix of X depending on the nonsingular integrals of the Erdogan fundamental solution multiplied by the B-spline function and the displacement interpolation function.

Substituting Eqs. (14) and (15) into Eq. (18), one obtains a relationship between the nodal force vector and the nodal displacement vector for the cracked superelement shown in Fig. 2, which can be written as

$$F_e = K_e U_e, \tag{19}$$

where K_e is the stiffness matrix of the cracked superelement, which can be expressed as

$$K_e = A_F (A_U^T A_U)^{-1} A_U^T H. \tag{20}$$

It is worth noting that, due to the possible numerical errors induced by SFBEM, the stiffness matrix obtained in Eq. (20) may be slightly asymmetric. The matrix can be made symmetric by minimizing the square of the errors in the nonsymmetric off-diagonal terms [20], which yields

$$\tilde{K}_e = \frac{1}{2}(K_e + K_e^T). \tag{21}$$
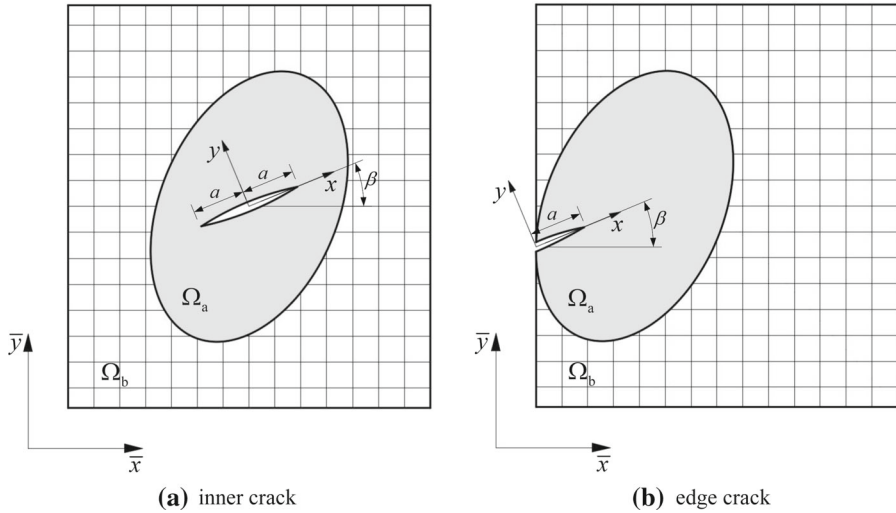
(a) inner crack   **(b)** edge crack

Fig. 3 Illustration of finite element mesh of plane domain with a cracked superelement

To reflect the degree of asymmetry of matrix $\boldsymbol{K}_e$, define the asymmetry index as follows:

$$\varepsilon = \frac{\left\| \tilde{\boldsymbol{K}}_e - \boldsymbol{K}_e \right\|_2}{\| \boldsymbol{K}_e \|_2} \times 100\%, \tag{22}$$

where $\|\cdot\|_2$ denotes the L_2 norm of matrix. In general, when the asymmetry index ε is smaller than 5%, the stiffness matrix $\boldsymbol{K}_e$ of the cracked superelement will sufficiently approach to a symmetric matrix, indicating the accuracy of SFBEM in the formulation of the superelement.

3 Analysis of crack problems by SFBEM–FEM coupling method

Now that the stiffness matrix of the cracked superelement has been formulated with SFBEM, it can be further assembled to the global FEM formulation for analysis of the entire structure. After global finite element analysis, the SIFs of the cracked superelement can be finally obtained by a backward analysis using SFBEM.

3.1 FEM formulation with cracked superelement

Consider a plane domain with an inner crack or an edge crack, as shown in Fig. 3, in which the near-crack region Ω_a is modelled with the cracked superelement Ω_e proposed in Sect. 2.2, and the rest region Ω_b is modelled using traditional finite elements. As the stiffness matrix of the cracked superelement is established under the local coordinate system $x-y$, it should be transformed to the form under the global coordinate

system $\bar{x}-\bar{y}$ shown in Fig. 3, which can be expressed as

$$\bar{K}_e = T^T \tilde{K}_e T, \tag{23}$$

where $\tilde{K}_e$ is the stiffness matrix of the cracked superelement under the local coordinate system $x-y$, which has been obtained in Eqs. (20) and (21) by SFBEM; $\bar{K}_e$ is the stiffness matrix of the cracked superelement under the global coordinate system $\bar{x}-\bar{y}$; and T is the coordinate transformation matrix, which can be written as

$$T = \begin{bmatrix} T_1 & 0 & \cdots & 0 \\ 0 & T_2 & & \vdots \\ \vdots & & \ddots & 0 \\ 0 & \cdots & 0 & T_N \end{bmatrix}, \tag{24}$$

where

$$T_n = \begin{bmatrix} \cos\beta & \sin\beta \\ -\sin\beta & \cos\beta \end{bmatrix} \quad (n = 1, 2, \ldots, N), \tag{25}$$

where N is the number of the nodes of the cracked superelement; and β is the angle between the x-axis and the $\bar{x}$-axis, as shown in Fig. 3.

Suppose that, under the global coordinate system $\bar{x}-\bar{y}$, the displacement vector of the nodes of the cracked superelement is U_a, while the displacement vector of the rest nodes of the finite element mesh is U_b. The external force vectors are assumed to be F_a and F_b corresponding to U_a and U_b, respectively. Then, following the typical procedure of finite element analysis, the global stiffness equation can be obtained as

$$KU = F, \tag{26}$$

where $U = [U_a^T U_b^T]^T$, $F = [F_a^T F_b^T]^T$; and K is the global stiffness matrix, which is expressed as

$$K = \begin{bmatrix} K_{aa} + \bar{K}_e & K_{ab} \\ K_{ba} & K_{bb} \end{bmatrix}, \tag{27}$$

where $\bar{K}_e$ is the stiffness matrix of the cracked superelement shown in Eq. (23); and K_{aa}, K_{ab}, K_{ba} and K_{bb} are the block stiffness matrices contributed by the traditional finite elements.

Note that, for a multi-crack problem, multiple cracked superelements need to be employed to model different near-crack regions, and the global stiffness equation can be formulated as above by merging different superelements to the traditional finite elements.

3.2 SIF analysis of cracked superelement

After solving for the global displacement vector $U = [U_a^T U_b^T]^T$ from Eq. (26), a backward analysis with SFBEM is required for the SIF analysis of the cracked superelement. For this purpose, the nodal displacement vector U_e of the cracked superelement under local coordinate system $x-y$ is first obtained from U_a by coordinate transformation as follows:

$$U_e = T U_a, \tag{28}$$

where T is the coordinate transformation matrix shown in Eq. (24).

Substituting Eq. (28) into Eq. (14) and considering Eq. (15), the vector of spline node parameters of the fictitious loads can then be obtained as

$$X = (A_U^T A_U)^{-1} A_U^T H T U_a. \tag{29}$$

On the other hand, under the action of the fictitious loads $X^{(k)} (k = 1, 2)$, the mode-I and mode-II SIF at the crack tips of the cracked superelement shown in Fig. 2 can be directly obtained as

$$\left. \begin{array}{l} K_I = \sum\limits_{k=1}^{2} \int_S G_{K_I}^{(k)}(z_S) X^{(k)}(z_S) ds \\ K_{II} = \sum\limits_{k=1}^{2} \int_S G_{K_{II}}^{(k)}(z_S) X^{(k)}(z_S) ds \end{array} \right\}, \tag{30}$$

where $G_{K_I}^{(k)}$ and $G_{K_{II}}^{(k)} (k = 1, 2)$ are the Erdogan SIF fundamental solutions presented in Sect. 2.1.

Using Eq. (10), the discretization form of Eq. (30) can be derived as

$$K_{SIF} = A_K X, \tag{31}$$

where $K_{SIF} = [K_I K_{II}]^T$ is the SIF vector of the cracked superelement; X is the vector of spline node parameters of the fictitious loads; and A_K is the influence matrix of X depending on the integrals of the Erdogan SIF fundamental solution multiplied by the B-spline function.

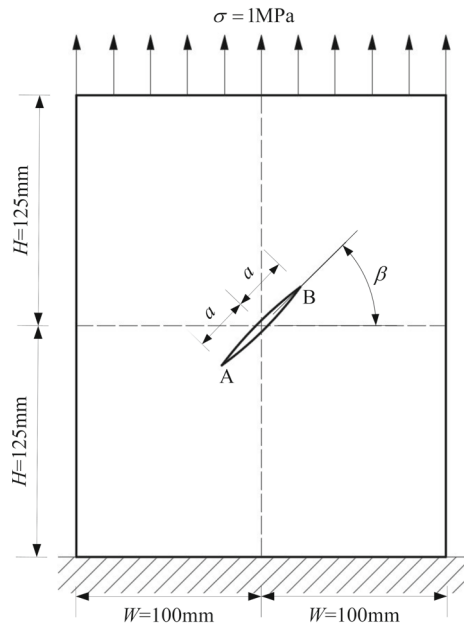Substitution of Eq. (29) into Eq. (31) yields

$$K_{SIF} = B U_a, \tag{32}$$

where

$$B = A_K (A_U^T A_U)^{-1} A_U^T H T. \tag{33}$$

Note that, as the fundamental solutions of SIFs are available in the formulation, the SIFs of the crack tips can be directly obtained via Eq. (32) from the nodal displacements

of the cracked superelement, with no need of transformation from the displacement field around the crack tip, which is generally required in SIF analysis with the other numerical methods. This further leads to the high efficiency and accuracy of the present approach.

4 Numerical examples

To validate the accuracy and efficiency of the proposed SFBEM–FEM coupling method, the cracked superelements formulated with SFBEM are incorporated into the commercial FEM software Abaqus with the help of the user-defined elements [30]. Two numerical examples for SIF analysis of a rectangular plate with a central inclined crack and a square plate with 100 horizontal cracks are considered in this section. The finite element meshes for these two examples are generated with the meshing techniques provided by Abaqus.

4.1 A rectangular plate with a central inclined crack

Consider a rectangular plate with one side fixed and the opposite side subjected to a uniform tensile load $\sigma = 1$ MPa, as shown in Fig. 4. The modulus of elasticity and Poison's ratio of the plate are taken as $E = 1000$ MPa and $\upsilon = 0.2$, respectively, and the width and height of the plate are assumed to be $2W = 200$ mm and $2H = 250$ mm, respectively. An inclined crack AB is located at the centre of the plate, whose length and inclined angle are $2a$ and β, respectively, as also shown in Fig. 4.
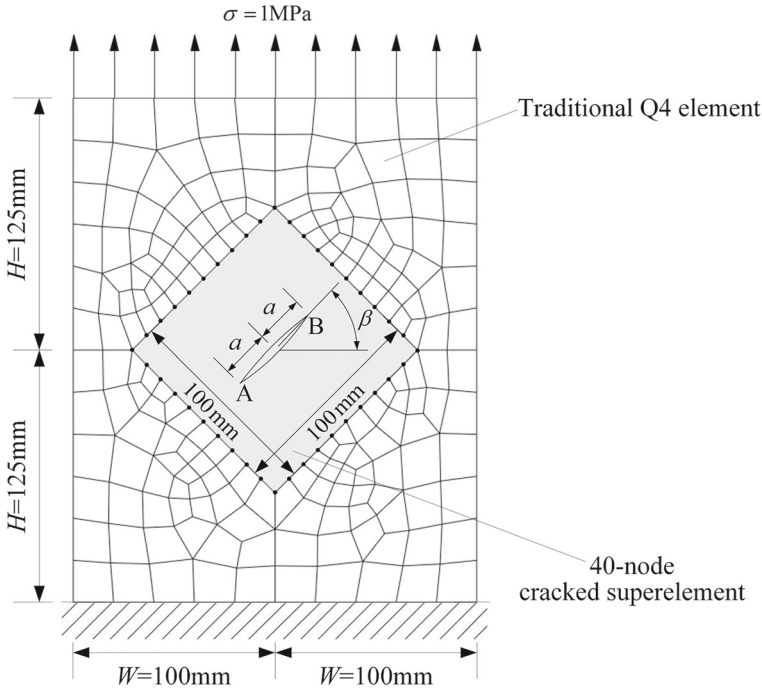
Fig. 5 Finite element mesh consisting of a superelement and 192 Q4 elements ($\beta = 45^\circ$)

The crack problem shown in Fig. 4 is solved with the proposed SFBEM–FEM coupling method, in which the near-crack region is modelled using a 100 mm × 100 mm superelement with the crack located at the centre, and the other region is discretized with traditional Q4 plate elements. In particular, when $\beta = 45°$, the mesh consists of a superelement and 192 Q4 elements, which is shown in Fig. 5. For the cracked superelement, a total of 40 nodes have been adopted, and 40 fictitious boundary elements and 80 boundary segments are employed in calculating the stiffness matrix of the 40-node superelement with the distance between the real boundary and the fictitious boundary being taken as the length of the boundary segment, i.e. $d = 5$ mm. It has been observed that the asymmetry index ε defined in Eq. (22) is just around 4.62% using the above parameters, and thus the accuracy of the proposed method can be guaranteed regarding the formulation of the superelement. For comparison, the crack problem is also analysed using the traditional FEM with Abaqus, in which, to obtain the reference solution, the near-crack region is discretized into a sufficiently fine mesh leading to a total number of 1748 Q4 elements for the entire problem ($a/W = 0.3$), as shown in Fig. 6. Comparing the finite element meshes shown in Figs. 5 and 6, it can be seen that the number of DOFs involved in the coupling method is much smaller than that of the traditional FEM due to the use of the cracked superelement. Furthermore, for a given value of β, the coupling mesh shown in Fig. 5 remains the same for different crack lengths, while for the domain shown in Fig. 6, it needs to be remeshed when the crack length changes.
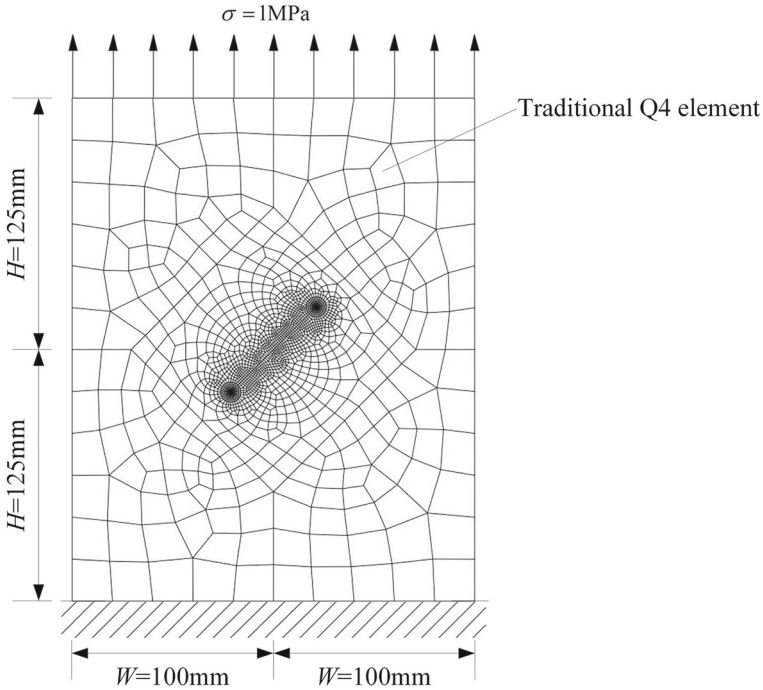
Fig. 6 Finite element mesh consisting of 1748 Q4 elements ($\beta = 45°$, $a/W = 0.3$)

Table 1 The results of K_I and K_{II} of crack tip A with $\beta = 0°$ and $\beta = 45°$

| β (°)	a/W	K_I (MPa · mm$^{1/2}$)		Deviation (%)	K_{II} (MPa · mm$^{1/2}$)		Deviation (%)
		Coupling method	Traditional FEM		Coupling method	Traditional FEM	
0	0.1	5.7075	5.7083	−0.0140	–	–	–
	0.2	8.2300	8.2414	−0.1383	–	–	–
	0.3	10.4163	10.4522	−0.3435	–	–	–
45	0.1	2.8781	2.8638	0.4993	2.8449	2.8397	0.1831
	0.2	4.2187	4.1659	1.2674	4.0815	4.0866	−0.1248
	0.3	5.4160	5.3376	1.4688	5.0854	5.0617	0.4682

   When $\beta = 0°$ and $\beta = 45°$, the SIFs K_I and K_{II} of crack tips A and B corresponding to different crack lengths are presented in Tables 1 and 2, respectively, from which it can be seen that the results of the SFBEM–FEM coupling method agree well with those of the traditional FEM with relative deviations being less than 1.5%, indicating the high accuracy of the present method. To investigate the variation of K_I and K_{II} with the inclined angle β under different ratios of the crack length to plate width, a/W, the results are depicted in Figs. 7 and 8 for crack tips A and B, respectively. It can be observed from the above figures that K_I decreases with the increase of β for both crack tips. While for K_{II}, it will first increase with the increase of β until $\beta = 45°$,

Table 2 The results of K_I and K_{II} of crack tip B with $\beta = 0°$ and $\beta = 45°$

β (°)	a/W	K_I (MPa · mm$^{1/2}$)		Deviation (%)	K_{II} (MPa · mm$^{1/2}$)		Deviation (%)
		Coupling method	Traditional FEM		Coupling method	Traditional FEM	
0	0.1	5.7067	5.7080	−0.0234	–	–	–
	0.2	8.2288	8.2405	−0.1414	–	–	–
	0.3	10.4116	10.4494	−0.3621	–	–	–
45	0.1	2.8675	2.8533	0.4989	2.8481	2.8433	0.1696
	0.2	4.1961	4.1500	1.1108	4.0927	4.0729	s 0.4861
	0.3	5.4019	5.3283	1.3813	5.1099	5.0943	0.3062

Fig. 7 The SIFs of crack tip A with different values of β and a/W
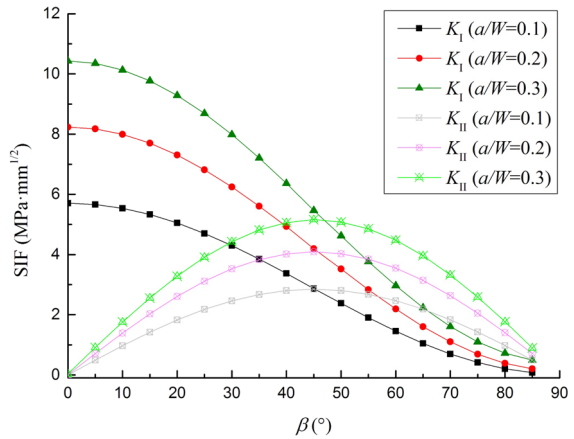
and then it will drop with further increase of β. It can be further observed from Figs. 7 and 8 that both K_I and K_{II} increase with the increase of a/W under a specific value of β.

To investigate the influence on the results of the proposed SFBEM–FEM coupling method, different values of the distance d between the real boundary and the fictitious boundary are taken in calculating the stiffness matrix of the cracked superelement for the case of $\beta = 45°$ and $a/W = 0.2$. The results are presented in Tables 3 and 4, from which it can be observed that the distance between the fictitious boundary and the real boundary can be changed in a reasonable range with little influence on the results, indicating the numerical stability of the present method. As a general rule, the distance between the fictitious boundary and the real boundary in SFBEM should be taken as the same order of magnitude of the length of the real boundary segments. This conclusion has also been drawn in the previous study reported in [11, 27]. Detailed investigation on the optimal location of the fictitious boundary can be found in [31].

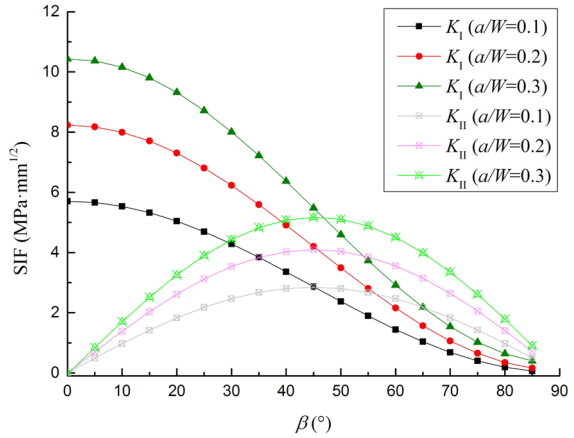**Fig. 8** The SIFs of crack tip B with different values of β and a/W

Table 3 The results of K_I and K_{II} of crack tip A with different values of distance d ($\beta = 45°$ and $a/W = 0.2$)

SIF (MPa · mm$^{1/2}$)	Traditional FEM	Coupling method				
		$d =3$mm	$d =4$mm	$d =5$mm	$d =6$mm	$d =7$mm
K_I	4.1659	4.2253	4.2227	4.2187	4.2225	4.2246
K_{II}	4.0866	4.0846	4.0824	4.0815	4.0823	4.0825

Table 4 The results of K_I and K_{II} of crack tip B with different values of distance d ($\beta = 45°$ and $a/W = 0.2$)

SIF (MPa · mm$^{1/2}$)	Traditional FEM	Coupling method				
		$d =3$ mm	$d =4$ mm	$d =5$ mm	$d =6$ mm	$d =7$ mm
K_I	4.1500	4.2015	4.1998	4.1961	4.1995	4.2017
K_{II}	4.0729	4.0943	4.0941	4.0927	4.0940	4.0942

4.2 A square plate with 100 horizontal cracks

Consider a square plate containing $10 \times 10 = 100$ equally spaced horizontal cracks, as shown in Fig. 9. The length of each crack is taken to be $2a = 40$ mm. The plate is fixed at the bottom side and is subjected to a uniform tensile load $\sigma = 1$ MPa at the top side. The modulus of elasticity and Poison's ratio of the plate are assumed to be $E = 200$ GPa and $\upsilon = 0.25$, respectively, and the width and height of the plate are assumed to be $2W = 3000$ mm and $2H = 3000$ mm, respectively.

The crack problem is solved with the proposed SFBEM–FEM coupling method, in which the plate domain is discretized with $10 \times 10 = 100$ cracked superelements, as shown in Fig. 9. The width and height of each superelement are $2w = 300$ mm and $2h = 300$ mm, respectively, and the crack is located at the centre of the superelement. To obtain the SIF results with sufficient accuracy, a total of 40 nodes are adopted for each superelement, and 40 fictitious boundary elements and 80 boundary segments
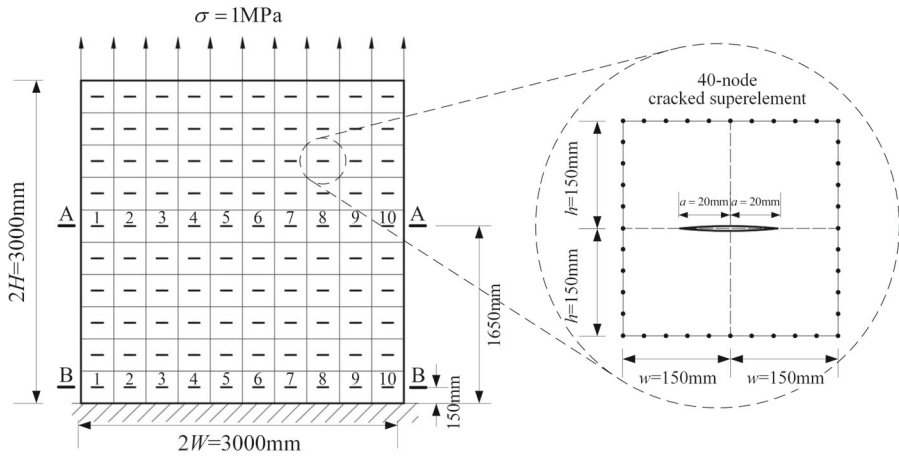
Fig. 9 A square plate with $10 \times 10 = 100$ equally spaced horizontal cracks and the finite element mesh consisting of $10 \times 10 = 100$ cracked superelements

are employed in calculating the stiffness matrix of the superelement with the distance between the real boundary and the fictitious boundary being taken as the length of the boundary segment, i.e. $d = 15$ mm. The asymmetry index ε defined in Eq. (22) has been found to be just 3.73% with the above parameters, indicating the accuracy of the proposed method regarding the formulation of the superelement. Note that, for this particular problem, as the $10 \times 10 = 100$ cracked superelements have covered the whole domain of the plate, no traditional finite elements are required in the present approach. For comparison, the crack problem is also analysed using the traditional FEM with Abaqus, in which a total number of 140539 Q4 elements need to be used for obtaining the reference solution of the problem, as shown in Fig. 10. Obviously, the number of DOFs involved in the coupling method with the mesh shown in Fig. 9 is greatly reduced compared with that of the traditional FEM using the mesh shown in Fig. 10, and it is much easier to prepare for the mesh shown in Fig. 9 than that shown in Fig. 10.

To investigate the variation of the SIFs of the cracks located at the same horizontal section of the plate, sections A–A and B–B are taken into consideration with the cracks being numbered from 1 to 10, as shown in Fig. 9. Consider the left tips of the above cracks, and the values of K_I for different cracks at sections A–A and B–B are shown in Figs. 11 and 12, respectively, from which it can be seen that the results obtained with the SFBEM–FEM coupling method and the traditional FEM are in good agreement with the relative deviations being less than 0.5%, indicating the high accuracy of the proposed method. It can be also observed from the above figures that, at section A–A, the values of K_I range from 7.7905 to 8.0734 MPa $\cdot$ mm$^{1/2}$ with those of the cracks on both sides of the plate being a bit smaller, while at section B–B, the values of K_I range from 7.6157 to 8.9169 MPa $\cdot$ mm$^{1/2}$ with those of the cracks on both sides of the plate being significantly larger. Note that, for this particular example, the computing CPU time required by the coupling method is only 9.1% of that required by the FEM alone for solving the final system of equations.
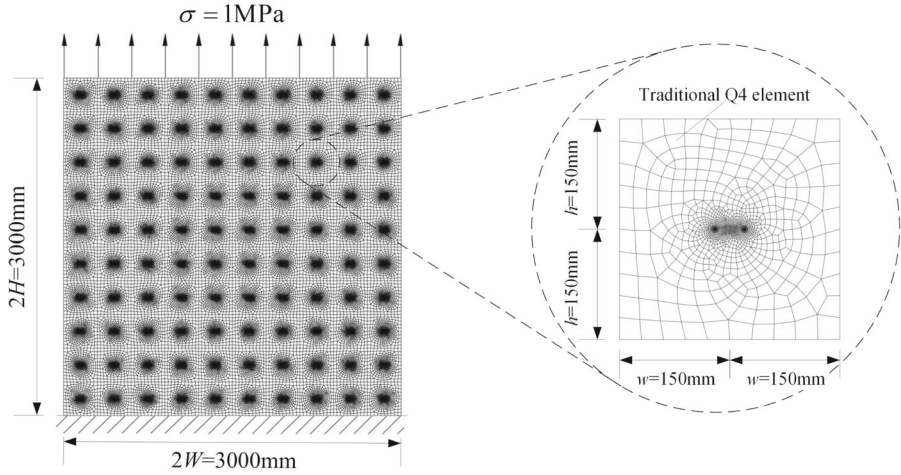
Fig. 10 Finite element mesh consisting of 140539 Q4 elements

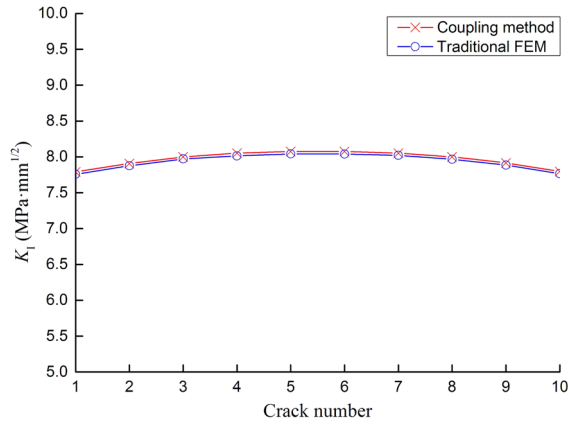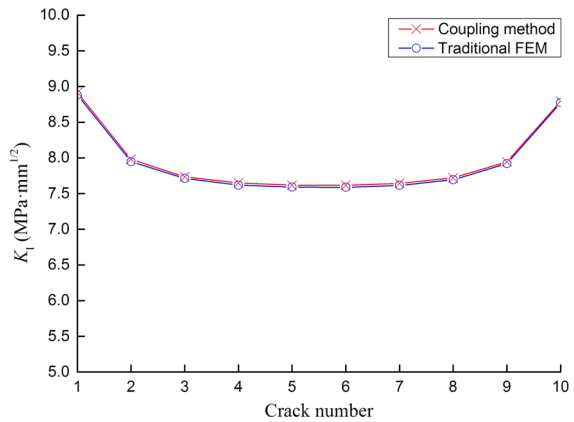**Fig. 11** The values of K_I for different cracks at section A–A

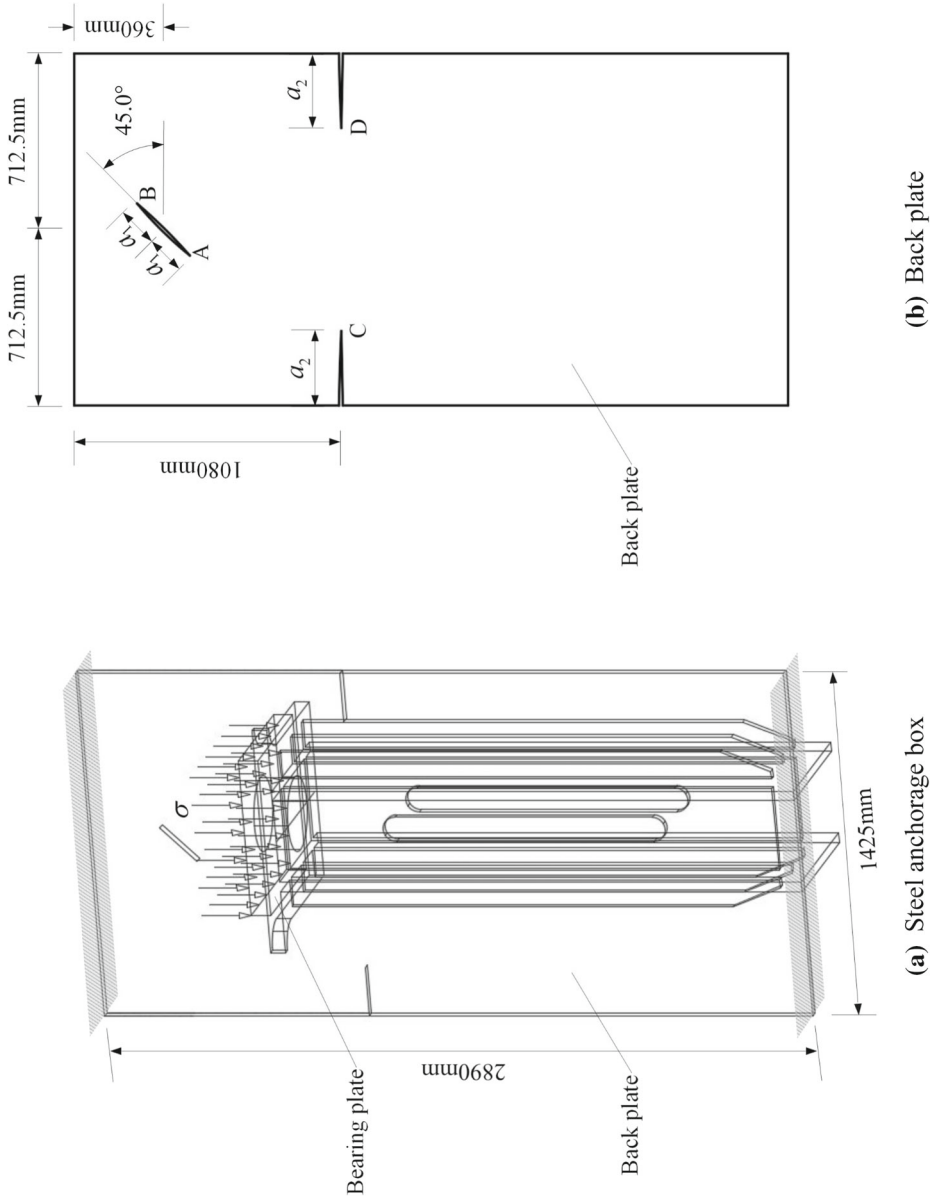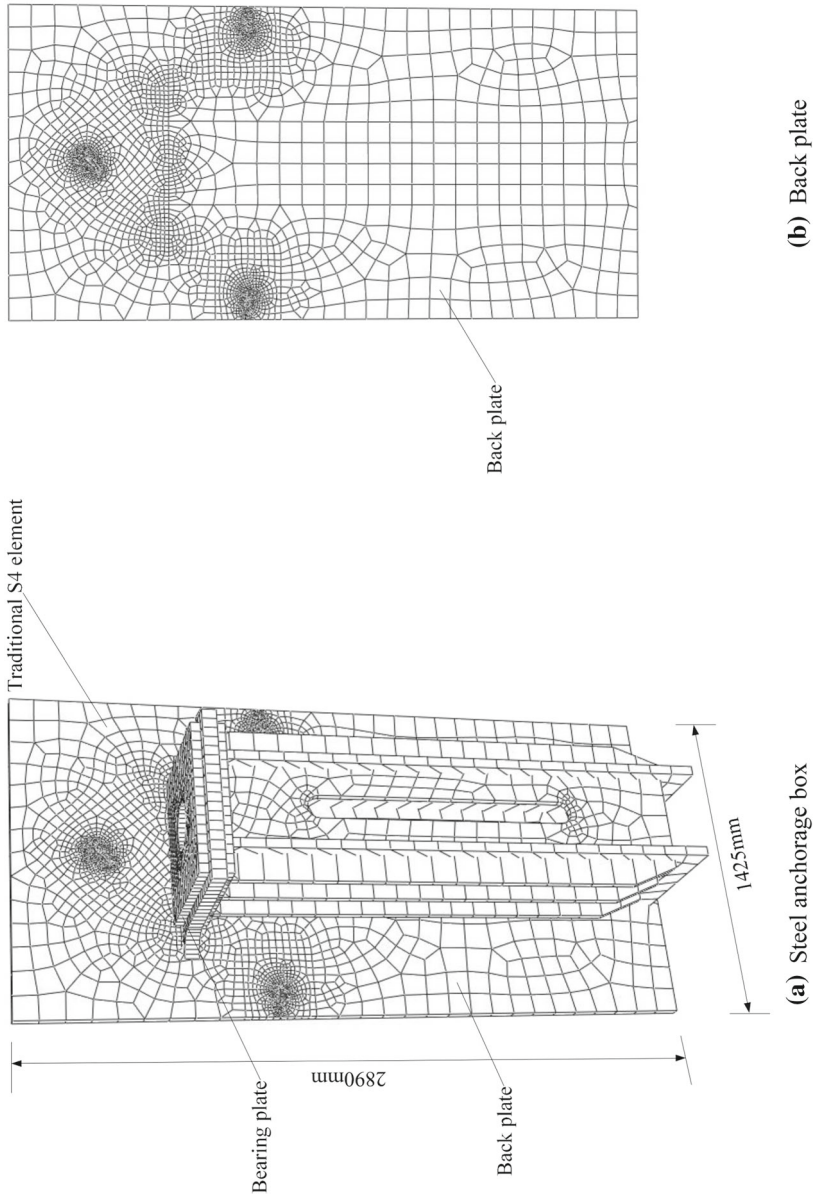**Fig. 12** The values of K_I for different cracks at section B–B

(b) Back plate

360mm

712.5mm

712.5mm

1080mm

45.0°

a_2

a_2

A

B

C

D

Back plate

(a) Steel anchorage box

1425mm

2890mm

σ

Bearing plate

Back plate

Fig. 13 A steel anchorage box with three cracks

(b) Back plate

Back plate

Traditional S4 element

Bearing plate

2890mm

1425mm

Back plate

(a) Steel anchorage box

Fig. 14 Finite element mesh consisting of 6404 S4 elements

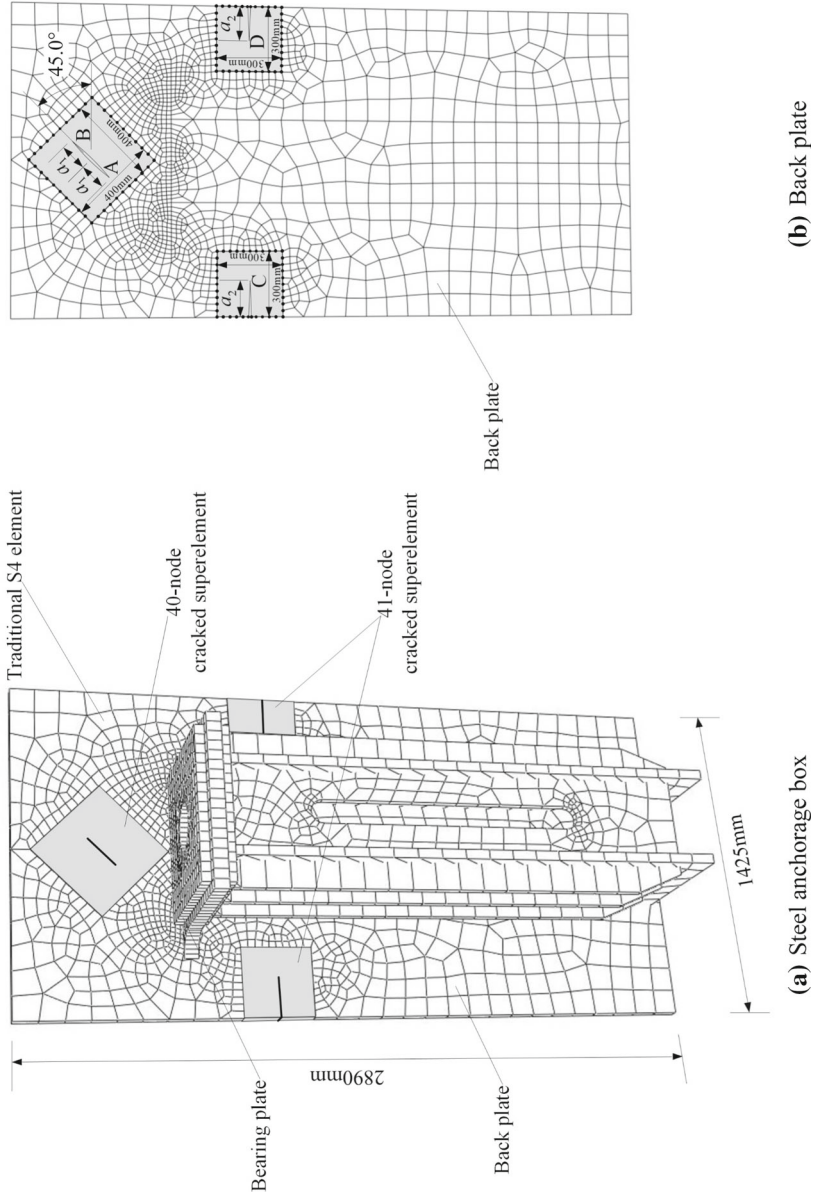**(b)** Back plate

(a) Steel anchorage box

Fig. 15 Finite element mesh consisting of three superelements and 2601 S4 elements

5 Engineering application

Crack propagation of the steel anchorage box for a hanger of a suspension bridge often occurs under the action of vehicle loads. The SIFs of cracks are important parameters for fatigue analysis of the steel anchorage box, and thus it is necessary to conduct the SIF analysis of the structure. A steel anchorage box is shown in Fig. 13. The back plate of the structure is assumed to be fixed at the upper and lower edge with two side edges being free. The bearing plate of the structure is subjected to a uniform pressure with an amplitude of $\sigma = 1.4057$ MPa, which is transformed from the tension amplitude of a hanger rod under the action of vehicle loads. The modulus of elasticity and Poison's ratio of the steel anchorage box are assumed to be $E = 210$ GPa and $\upsilon = 0.3$, respectively. Suppose that, after field inspection, three cracks are detected at the back plate, including an inner crack and two edge cracks, as also shown in Fig 13. The lengths of the inner crack and the two edge cracks are assumed to be $2a_1 = 100$ mm and $a_2 = 100$ mm, respectively. In this section, the cracked superelements formulated with SFBEM are incorporated into the commercial FEM software Abaqus with the user-defined elements, and the finite element mesh is generated with the meshing techniques provided by Abaqus.

The crack problem shown in Fig. 13 is first solved with the traditional FEM using Abaqus. To obtain the reference solution, a total of 6404 S4 shell elements are adopted for the analysis, and the finite element mesh is shown in Fig. 14. To validate the applicability of the present approach to engineering practice, the problem is also analysed with the SFBEM–FEM coupling method. The near-crack regions are modelled using one 400 mm × 400 mm centre-cracked superelement and two 300 mm × 300 mm edge-cracked superelements. To keep the superior flexibility of FEM in modelling the complex structure, the other region is discretized with 2601 traditional S4 elements. The coupling mesh is shown in Fig. 15. For the centre-cracked superelement, a total of 40 nodes have been adopted, and 40 fictitious boundary elements and 80 boundary segments are employed in calculating the stiffness matrix with the distance between the real boundary and the fictitious boundary being taken as $d = 20$ mm. For the edge-cracked superelement, a total of 41 nodes have been employed, and 60 fictitious boundary elements and 120 boundary segments are adopted in the formulation of the stiffness matrix, in which the distance between the real boundary and the fictitious boundary is taken as $d = 6$ mm. It can be found that, using the above parameters, the values of the asymmetry index ε defined in Eq. (22) are only 3.88% and 4.57% for the centre-cracked and the edge-cracked superelement, respectively, indicating the accuracy of SFBEM in calculating the stiffness matrices of the superelements.

The results of K_I and K_{II} for the crack tips A, B, C and D obtained by the coupling method and the traditional FEM are presented in Table 5. It can be seen from Table 5 that the results of the coupling method agree well with those of the traditional FEM. The relative deviations of the coupling method are less than 1.3%, indicating the high accuracy of the present approach. Note that, for this example, the elapsed CPU time of the coupling method is only 37.5% of that required by the FEM alone for solving the final system of equations.

Table 5 The results of K_I and K_{II} of crack tips with $2a_1 = 100\,\text{mm}$ and $a_2 = 100\,\text{mm}$

Crack tip	SIF	SIF value (MPa $\cdot$ mm$^{1/2}$)		Deviation (%)
		Coupling method	Traditional FEM	
A	K_I	33.0146	32.6479	1.1232
	K_{II}	32.1911	31.8732	0.9974
B	K_I	31.5570	31.1602	1.2734
	K_{II}	31.3420	31.0215	1.0332
C	K_I	19.1515	19.0432	0.5687
	K_{II}	-3.7738	-3.7307	1.1553
D	K_I	19.4107	19.3338	0.3977
	K_{II}	3.8416	3.8100	0.8294

6 Conclusions

To make full use of the unique advantage of SFBEM in dealing with the singular behaviour at crack tips while keeping the wide applicability of FEM in modelling complex structures and boundary conditions, this paper presents a SFBEM–FEM coupling method for the SIF analysis of complex crack problems. The stiffness matrix of the cracked superelement is first formulated by SFBEM based on the Erdogan fundamental solutions, in which the stress boundary conditions on the crack surfaces are automatically satisfied and the singular behaviour at crack tips can be naturally captured. Then, the proposed cracked superelements are incorporated into a finite element mesh to simulate the behaviour of different crack zones, and the global finite element equations are established and solved following the typical FEM procedure. Finally, the SIFs of the crack tips can be directly obtained by a backward analysis with SFBEM by superposition of the analytical SIF fundamental solutions, which are included as a part of the Erdogan fundamental solutions. Two numerical examples as well as an engineering application are presented to show the efficacy of the present approach by merging of the cracked superelements to the commercial FEM software. However, it should be pointed out that the present study is only limited to two-dimensional crack analysis. The coupling method for three-dimensional crack problems will be further considered in future study.

Declarations

Conflict of interest On behalf of all authors, the corresponding author states that there is no conflict of interest.

References

1. Shen DW, Fan TY (2003) Exact solutions of two semi-infinite collinear cracks in a strip. Eng Fract Mech 70(6):813–822

2. Busari YO, Ariri A, Manurung YH, Sebayang D, Leitner M, Zaini WS, Kamilzukairi MA, Celik E (2020) Prediction of crack propagation rate and stress intensity factor of fatigue and welded specimen with a two-dimensional finite element method. Mater Sci Eng 834(1):12008

3. Shi JX, Chopp D, Lua J, Sukumar N, Belytschko T (2010) Abaqus implementation of extended finite element method using a level set representation for three-dimensional fatigue crack growth and life predictions. Eng Fract Mech 77(14):2840–2863

4. He D, Guo Z, Ma H (2021) Penny-shaped crack simulation with a single high order smooth boundary element. Eng Anal Bound Elem 124:211–220

5. Belytschko T, Gracie R, Ventura G (2009) A review of extended/generalized finite element methods for material modeling. Modell Simul Mater Sci Eng 17(4):043001

6. De Luycker E, Benson DJ, Belytschko T, Bazilevs Y (2011) X-FEM in isogeometric analysis for linear fracture mechanics. Int J Numer Methods Eng 87(6):541–565

7. Banerjee PK, Butterfield R (1981) Boundary element methods in engineering science. McGraw-Hill, London, p 451P

8. Xie GZ, Zhang DH, Meng FN, Du W, Zhang J (2017) Calculation of stress intensity factor along the 3D crack front by dual BIE with new crack front elements. Acta Mech 228(9):3135–3153

9. Gu Y, Zhang CZ (2020) Novel special crack-tip elements for interface crack analysis by an efficient boundary element method. Eng Fract Mech 239:107302

10. Erdogan F (1962) On the stress distribution in a plate with collinear cuts under arbitrary loads. Proceedings of the 4th U.S. National Congress of Applied Mechanics, pp 547–553

11. Su C, Zheng C (2012) Probabilistic fracture mechanics analysis of linear-elastic cracked structures by spline fictitious boundary element method. Eng Anal Bound Elem 36(12):1828–1837

12. Xu Z, Su C, Guan ZW (2018) Analysis of multi-crack problems by the spline fictitious boundary element method based on Erdogan fundamental solutions. Acta Mech 229(8):3257–3278

13. Xu Z, Chen M, Su C (2019) Dynamic analysis of multi-crack problems by the spline fictitious boundary element method based on Erdogan fundamental solutions. Eng Anal Bound Elem 107:3257–3278

14. Frangi A, Novati G (2003) BEM-FEM coupling for 3D fracture mechanics applications. Comput Mech 32(4–6):415–422

15. Helldoerfer B, Haas M, Kuhn G (2008) Automatic coupling of a boundary element code with a commercial finite element system. Adv Eng Softw 39(8):699–709

16. Nikishkov G (2010) Combined finite- and boundary-element analysis of SCC crack growth. ISCMI Ii EPMESC Xii 1233:747–752

17. Rungamornrat J, Mear ME (2011) SGBEM-FEM coupling for analysis of cracks in 3D anisotropic media. Int J Numer Methods Eng 86(2):224–248

18. Nguyen TB, Rungamornrat J, Senjuntichai T, Wijeyewickrema AC (2015) FEM-SGBEM coupling for modeling of mode-I planar cracks in three-dimensional elastic media with residual surface tension effects. Eng Anal Bound Elem 55:40–51

19. Zienkiewicz OC, Kelly DW, Bettess P (1977) The coupling of the finite element method and boundary solution procedures. Int J Numer Methods Eng 11(2):355–375

20. Brebbia CA, Georgiou P (1979) Combination of boundary and finite elements in elastostatics. Appl Math Modell 3(3):212–220

21. Kim M (2021) A coupled formulation of finite and boundary element methods for flexoelectric solids. Finite Elem Anal Des 189:103526

22. Sharma N, Panda SK (2020) Multiphysical numerical (FE-BE) solution of sound radiation responses of laminated sandwich shell panel including curvature effect. Comput Math Appl 80(1):1221–1239

23. Huang H, Zou MS, Jiang LW (2019) Study of integrated calculation method of fluid-structure coupling vibrations, acoustic radiation, and propagation for axisymmetric structures in ocean acoustic environment. Eng Anal Bound Elem 106:334–348

24. Fu Z, Xi Q, Li Y, Huang H, Rabczuk T (2020) Hybrid FEM-SBM solver for structural vibration induced underwater acoustic radiation in shallow marine environment. Comput Methods Appl Mech Eng 369:113236

25. Gimperlein H, Oezdemir C, Stephan EP (2020) A time-dependent FEM-BEM coupling method for fluid-structure interaction in 3d. Appl Numer Math 152:49–65

26. Ai ZY, Chen YF (2020) FEM-BEM coupling analysis of vertically loaded rock-socketed pile in multilayered transversely isotropic saturated media. Comput Geotech 120:103437

27. Su C, Han DJ (2000) Multidomain SFBEM and its application in elastic plane problems. J Eng Mech ASCE 126(10):1057–1063

28. Su C, Zhao SW, Ma HT (2012) Reliability analysis of plane elasticity problems by stochastic spline fictitious boundary element method. Eng Anal Bound Elem. 36(2):118–124
29. Su C, Xu J (2015) Reliability analysis of Reissner plate bending problems by stochastic spline fictitious boundary element method. Eng Anal Bound Elem 51:37–43
30. Abaqus Analysis User's Manual, Version 6.13, 2013, Abaqus, Inc
31. Cheng AHD, Hong YX (2020) An overview of the method of fundamental solutions-Solvability, uniqueness, convergence, and stability. Eng Anal Bound Elem 120:118–152